






Magnon diffusion lengths in bulk and thin film Fe₃O₄ for spin Seebeck applicationsG. Venkat ^{1,*} C. D. W. Cox ¹ D. Voneshen ² A. J. Caruana ² A. Piovano,³ M. D. Cropper,¹ and K. Morrison ¹¹*Department of Physics, Loughborough University, Loughborough, LE11 3TU, United Kingdom*²*ISIS Neutron and Muon Source, Didcot, Oxfordshire, OX11 0QX, United Kingdom*³*Institut Laue-Langevin, 6 rue Jules Horowitz, 38042 Grenoble Cedex 9, France*

(Received 13 February 2020; revised 13 May 2020; accepted 16 June 2020; published 10 July 2020)

The magnon diffusion length (MDL) is understood to play a major role in the thickness dependence of spin Seebeck effect (SSE) voltages in Fe₃O₄/Pt thin films. Here we extract the MDL in an Fe₃O₄ single crystal using inelastic neutron scattering (INS) and in Fe₃O₄/Pt thin films using accurate heat flux SSE and static magnetization measurements. The INS MDLs were 34 ± 8 nm at 300 K and 27 ± 6 nm at 50 K. The SSE MDLs decreased with temperature (19 ± 2 nm at 300 K and 13 ± 4 nm at 50 K), but were markedly smaller. Whilst the bulk MDL is expected to be an upper limit of the MDL in thin films, we show that the film magnetization must be considered to obtain MDLs from SSE measurements. This study highlights the importance of disentangling the role of various effects in SSE measurements which is crucial in increasing the efficiencies of thermomagnetic energy harvesting devices.

DOI: [10.1103/PhysRevMaterials.4.075402](https://doi.org/10.1103/PhysRevMaterials.4.075402)

The spin Seebeck effect (SSE) was demonstrated in 2008 by Uchida *et al.* and has since sparked a lot of interest for potential thermoelectric applications [1]. In the longitudinal configuration [2], a spin current is generated along an applied temperature gradient which is normal to the magnetization. As spin currents cannot be detected easily, they are usually converted to charge currents in an adjacent metallic layer with high spin-orbit interaction (e.g., Pt) by the inverse spin Hall effect (ISHE) [2]. This discovery has paved the way for spin caloritronics that includes other thermomagnetic effects such as the spin Peltier and Nernst effects [3,4]. While the efficiency of conventional thermoelectrics is limited by the interplay of thermal (κ) and electric (σ) conductivities [5], the SSE is a candidate for improving the performance by allowing for the decoupling of κ and σ in the heavy metal and magnetic material [6]. The SSE is also a viable source of spin currents for spintronic applications [7,8].

Although the SSE was initially demonstrated in a metallic ferromagnet [1], it was later seen in the insulating ferrimagnet yttrium iron garnet (YIG) [9], which has become the benchmark material for SSE studies [2]. There have also been studies of the SSE in half metals such as Heusler alloys [10,11] and Fe₃O₄, which are particularly relevant to spintronic applications due to the theoretically proposed 100% spin polarization at the Fermi level [12]. As the oldest known magnetic

material, Fe₃O₄ has many technological applications [13] and has been attracting attention for SSE devices [14–17].

In an insulator, the SSE is driven by magnon propagation [18] as opposed to being driven by spin polarized conduction electrons in metallic systems [3]. In the former case and for low conductivity magnets like Fe₃O₄, an important length scale for quantifying the maximum SSE efficiency is the magnon diffusion length (MDL) Λ [19]. Quantitative knowledge of Λ is also useful for studying fundamentally new physics such as magnon Bose-Einstein condensates [20]. Kehlberger *et al.* extracted $\Lambda_{\text{YIG}} = 90\text{--}140$ nm from SSE measurements in YIG thin films, using an exponential model [21]. However, microwave measurements on YIG have found significantly larger MDLs ~ 400 nm [22]. In MgO/Fe₃O₄/Pt thin films, the MDL was extracted from SSE measurements using the linear response theory (LRT) [23] and found to be $\Lambda_{\text{Fe}_3\text{O}_4} = 17$ nm at 300 K, increasing to 40 nm at 70 K [14]. Since Fe₃O₄ seems to show a temperature dependence of the MDL affecting the spintronic efficiency and there is some discrepancy in the MDLs obtained (for YIG), a careful direct measurement of the MDL of Fe₃O₄ is required.

Another aspect of the SSE is its dependence on the saturation magnetization M_s . A decrease in SSE in bulk single-crystal YIG/Pt at 175 K has been correlated with an increase in magnetic surface anisotropy [24]. A similar decrease in the SSE in both bulk and thin films of YIG/Pt at 300 K at low magnetic fields has been attributed to the perpendicular magnetic anisotropy and its effect on the ISHE [25]. Thus, for comparing the SSE in different systems, we need to decouple the ISHE from the SSE and study the static magnetization and magnon propagation contributions separately.

In this paper, we measure the magnon dispersion and group velocity in single-crystal Fe₃O₄ using inelastic neutron scattering (INS). Subsequently, we fit integrated energy cuts of the magnon dispersion to simulated scattered neutron intensity

*Present address: Department of Materials Science and Engineering, University of Sheffield, Sheffield, S1 3JD, UK; guruvenkat7@gmail.com

Published by the American Physical Society under the terms of the [Creative Commons Attribution 4.0 International license](https://creativecommons.org/licenses/by/4.0/). Further distribution of this work must maintain attribution to the author(s) and the published article's title, journal citation, and DOI.

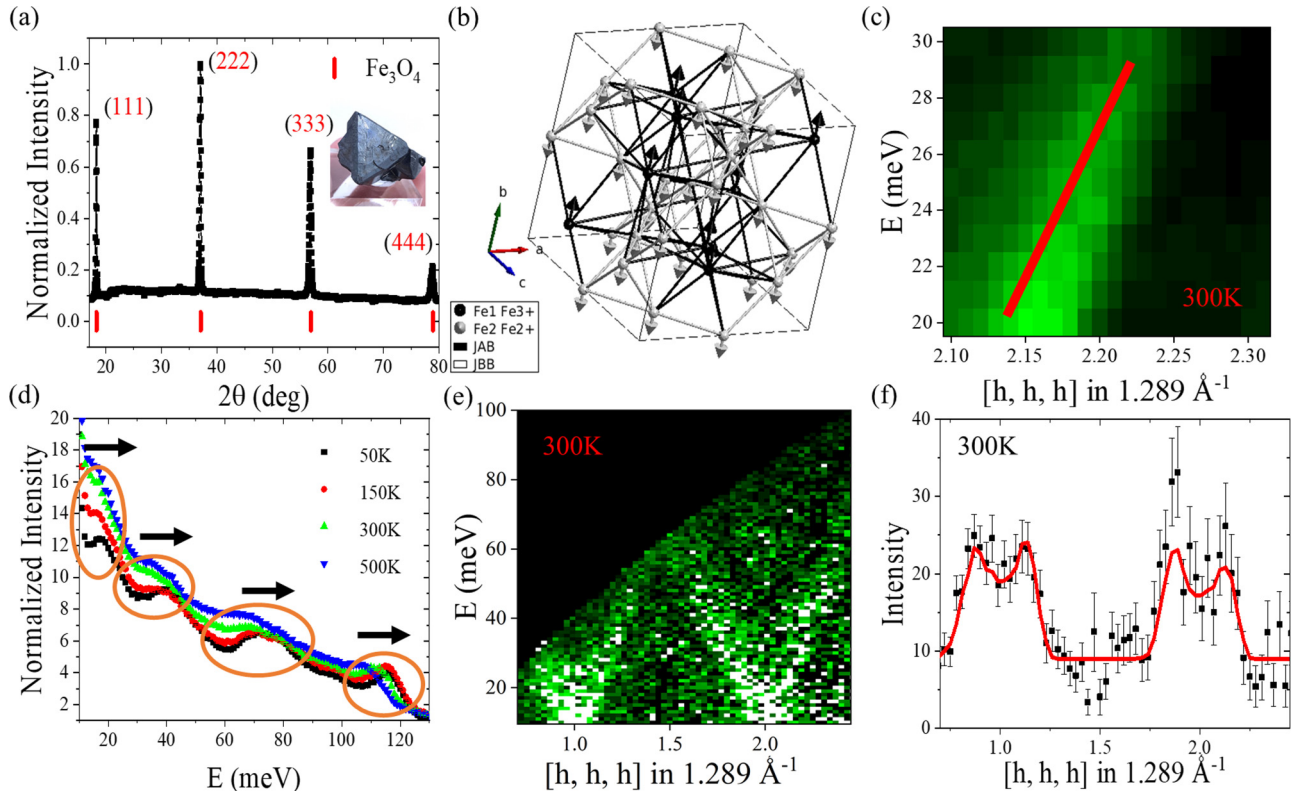


FIG. 1. (a) XRD spectrum of the single crystal showing the [111] orientation. The red dashes mark the positions of the [111] (and harmonics) obtained from the ICSD database (ICSD: 26410). The inset shows a portion of the single crystal used for the measurement. (b) The magnetic structure of Fe_3O_4 showing the different magnetic sites, antiferromagnetic exchange J_{AB} (light grey lines) and ferromagnetic exchange J_{BB} (black lines) interactions. (c) Magnon dispersion of Fe_3O_4 along the [222] direction at 300 K measured using TAS on IN8 at the ILL, Grenoble. The red line is a guide used to extract the group velocity. (d) Energy variation of scattered neutron intensity obtained from MAPS, integrated over all reciprocal space directions. The arrows indicate the blue shift of the magnon modes (marked by ellipses) with decreasing temperature (accompanied by narrowing of the spectra). (e) Magnon dispersion of Fe_3O_4 along the [HHH] direction at 300 K measured using TOF spectroscopy on MAPS at ISIS, UK. The almost linear variation of the dispersion is due to the antiferromagnetic exchange J_{AB} dominating in Fe_3O_4 . (f) A line cut along \mathbf{q} in Fig. 1(e) and integrated in energy from 20–30 meV. This was fit (shown in red) to the simulated scattered neutron intensity for the Fe_3O_4 magnetic structure and used to extract magnon linewidths.

profiles to obtain magnon linewidths and diffusion lengths at 300 and 50 K. We then report SSE measurements on Fe_3O_4 thin films at the same temperatures normalized to the heat flux $J_Q = Q/A$ (where Q is the heat passing through the sample and A is the sample area) passing through the film. We also measure the variation of the in-plane magnetization with Fe_3O_4 thickness and show that it mirrors the trend of the SSE coefficient. We proceed to normalize the SSE coefficient with the magnetization of the films to remove the static magnetization contribution to the measured SSE (introduced via the ISHE) and extract MDLs from the SSE measurements by fitting to the LRT [14] and exponential models [21]. We observe a decrease of the Fe_3O_4 MDL as the temperature is decreased, contrary to what was previously reported [14]. In addition, the MDL measured by INS is larger than that determined from SSE measurements, which could be a difference between bulk and thin film MDL values.

We initially used triple axis spectroscopy (TAS) using the IN8 instrument at the ILL, Grenoble to measure the magnon dispersion at 300 K. The measurement was performed on a 5-g naturally grown [111] oriented single crystal

of Fe_3O_4 , which was obtained from the Three Peaks mine in Utah, USA and is shown in the inset of Fig. 1(a). The XRD pattern in Fig. 1(a) shows the [111] orientation of the crystal. Since the magnon dispersion in Fe_3O_4 is isotropic along [001], [110], and [111] directions [26], measurement along the [111] is representative. Figure 1(b) shows the cubic inverse spinel structure of Fe_3O_4 with two different symmetry sites for the Fe ions: tetrahedral A sites occupied by Fe^{3+} ions and octahedral B sites populated by a random distribution of Fe^{2+} and Fe^{3+} ions. The antiferromagnetic exchange coupling between the ferromagnetic A and B sublattices results in the overall magnetic structure being ferrimagnetic. The magnetic exchange is well approximated by considering the antiferromagnetic exchange constant J_{AB} and the ferromagnetic exchange constant of the B sublattice J_{BB} [27]. Figure 1(c) shows the magnon dispersion along the [222] direction for the acoustic mode at 300 K from IN8 from which we obtained a magnon group velocity of $(14.63 \pm 0.80) \times 10^3$ m/s.

We then used time-of-flight (TOF) INS spectroscopy (on MAPS at the ISIS Neutron and Muon Source) to obtain the magnon dispersion at 50, 150, 300, and 500 K on the same

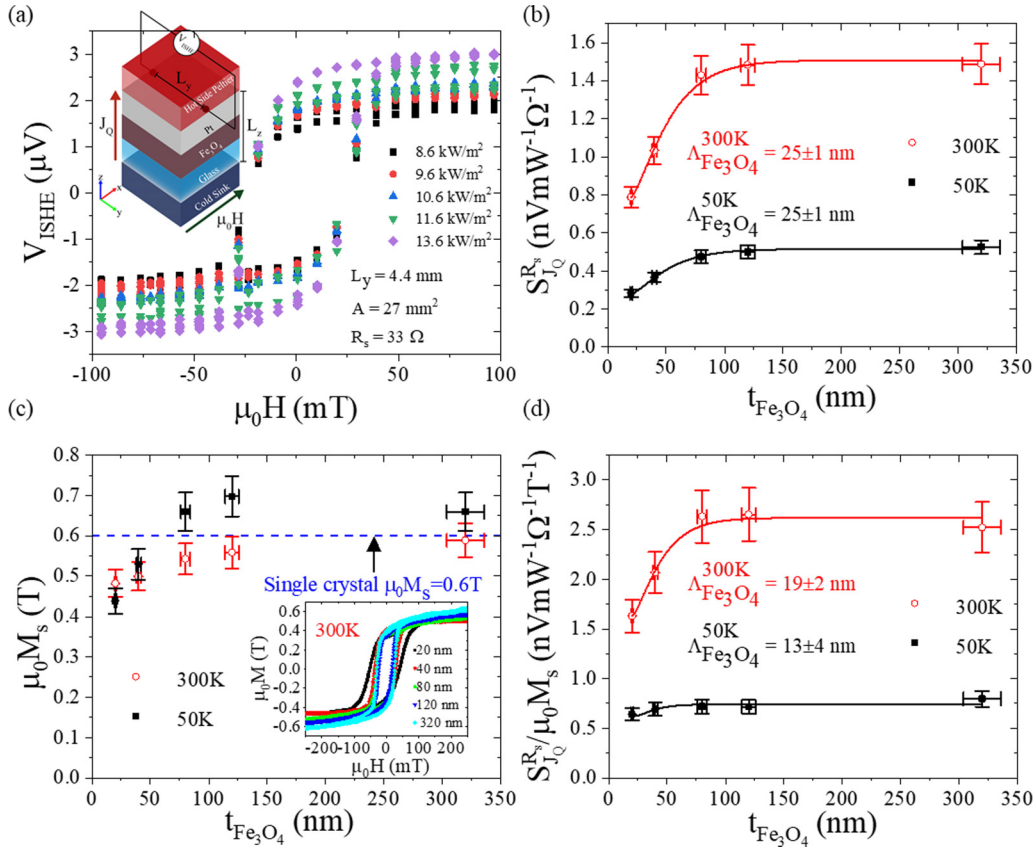


FIG. 2. (a) Example of the raw SSE voltage, V_{ISHE} , as a function of applied field $\mu_0 H$ for different heat fluxes J_Q at 300 K for the 80 nm film. The inset shows the schematic of the SSE measurement. (b) Variation of J_Q and sheet resistance normalized SSE coefficient $S_{J_Q}^{RS}$ with $t_{\text{Fe}_3\text{O}_4}$ at 50 and 300 K. The solid lines are fits obtained using Eq. (3). (c) The variation of the saturation magnetic flux density $\mu_0 M_s$ with $t_{\text{Fe}_3\text{O}_4}$ at 50 and 300 K. The dashed line marks the single-crystal value of $\mu_0 M_s$ for Fe_3O_4 . The inset shows the variation of the magnetic flux density $\mu_0 M$ with $\mu_0 H$ for the films of different $t_{\text{Fe}_3\text{O}_4}$ at 300 K. A linear diamagnetic background has been subtracted from the datasets. (d) Variation of $S_{J_Q}^{RS}/\mu_0 M_s$ with $t_{\text{Fe}_3\text{O}_4}$ at 50 and 300 K. The solid lines are fits obtained using Eq. (3).

sample. Figure 1(d) shows the scattered neutron intensity (integrated over $\mathbf{q} \in (-0.2, 0.2)$ r.l.u. in all directions in reciprocal space), as a function of temperature. The detected magnon modes occur as broad peaks in the spectrum and are marked by ellipses. A pronounced blue shift and decrease in magnon linewidth with temperature can be seen, which agrees well with simulated magnon spectrum in other ferrimagnetic systems such as YIG [28]. Figure 1 (e) shows the magnon dispersion along the [HHH] direction for the acoustic mode at 300 K. The dispersion slope gave a group velocity of $v_g^{300\text{ K}} = (13.97 \pm 1.82) \times 10^3$ m/s at 300 K. This is in good agreement with the group velocity extracted from the TAS IN8 measurement.

Subsequently, four cuts along the \mathbf{q} axis in Fig. 1(e) and integrated along energy (from 20–60 meV in four 10 meV ranges) were simultaneously fit (using the Tobyfit routine [29]) to the simulated scattered neutron intensity for the Fe_3O_4 magnetic structure (obtained using SPINW [30]). The fits, shown for the 20–30 meV cut in Fig. 1(f), gave an antiferromagnetic exchange constant of $J_{AB} = -4.49 \pm 0.01$ meV and a ferromagnetic exchange constant of $J_{BB} = 0.670 \pm 0.002$ meV, which agree well with literature [27]. We also extracted a linewidth of $\Gamma^{300\text{ K}} = 0.27 \pm 0.05$ meV, which corresponded to a magnon lifetime of $\tau^{300\text{ K}} = 2.44 \pm 0.45$ ps

at 300 K. Using $v_g^{300\text{ K}}$, we obtained a magnon diffusion length of $\Lambda_{\text{Fe}_3\text{O}_4}^{300\text{ K}} = v_g^{300\text{ K}} \tau^{300\text{ K}} = 34.1 \pm 7.7$ nm. Similarly, the magnon dispersion at 50 K, gave us $\Lambda_{\text{Fe}_3\text{O}_4}^{50\text{ K}} = 27.2 \pm 5.7$ nm. We thus observe that $\Lambda_{\text{Fe}_3\text{O}_4}$ is equal within error at 50 and 300 K. We regard these values obtained from bulk single-crystal measurements as upper limits on the MDL in Fe_3O_4 .

We now describe the SSE measurements. The samples investigated in this study were 5×5 mm² $\text{SiO}_2/\text{Fe}_3\text{O}_4/\text{Pt}$ thin films grown by pulsed laser deposition, with thicknesses $t_{\text{Fe}_3\text{O}_4} = 20, 40, 80, 120,$ and 320 nm and $t_{\text{Pt}} = 3\text{--}7.5$ nm with a preferential [111] texture [6]. More details of the sample characterization (including x-ray diffraction, reflectivity and fitting with GENX [31]) can be found in the SI [32] and in Ref. [6], while details of the SSE measurement setup is part of a manuscript which is under preparation [33]. Figure 2(a) shows example SSE measurements for the 80-nm film, where the raw voltage, V_{ISHE} , as the magnetic field $\mu_0 H$ was varied is plotted for different applied (and measured) J_Q . A schematic of the measurement configuration is also shown as an inset. The increase in V_{ISHE} with J_Q is due to the generated spin current being proportional to the temperature gradient, ∇T , across the Fe_3O_4 layer.

Since the SSE is usually associated with ∇T , the SSE coefficient is often defined (with units of V/K) as [34,35]

$$S_{\nabla T} = \frac{V_{\text{ISHE}} L_z}{L_y \Delta T}, \quad (1)$$

where L_y is the contact separation and L_z is the sample stack thickness. However, for thin films, it was shown by Sola *et al.* [36] that the thermal resistance between the sample and the hot and cold baths makes $S_{\nabla T}$ unreliable [35]. In addition, the limitation of ∇T measurements sampling the temperature difference across the substrate and active layers can result in stark differences between samples where the substrate thermal conductivity varies [6]. Instead, the SSE coefficient can be defined in terms of the heat flux J_Q (with units of Vm/W) as [36]

$$S_{J_Q} = \frac{V_{\text{ISHE}}}{L_y J_Q}, \quad (2)$$

where the direct relationship between J_Q and the temperature difference across the active layer is utilized. We thus consider J_Q normalization to define the SSE coefficient in this paper and note that $S_{\nabla T}$ can be obtained from S_{J_Q} by multiplying with the thermal conductivity of the magnetic layer.

An artefact that can contribute to the measured SSE response is the anomalous Nernst effect (ANE). The ANE has two possible contributions: (a) proximity magnetism induced in the Pt layer [37–39] and (b) the finite (but low) electrical conductivity of Fe_3O_4 . Since the Pt thickness in our films was larger than 3 nm, the proximity ANE was considered negligible [39,40]. The heat flux normalized ANE coefficient of a bare 80-nm-thick $\text{SiO}_2/\text{Fe}_3\text{O}_4$ film was measured to be $15.9 \pm 2.8 \text{ nVmW}^{-1}$ at 300 K. The resistance of the bare film was 756Ω while that of an 80-nm $\text{Fe}_3\text{O}_4/5 \text{ nm Pt}$ bilayer was 50Ω . Using the approach in [14], we obtained a corrected ANE response of $0.98 \pm 0.17 \text{ nVmW}^{-1}$, which is $<2.5\%$ of the SSE signal reported here. We therefore ignore the ANE. This is supported by measurements of Anadon *et al.* who found a negligible ANE contribution to the SSE signal ($\sim 7\%$) [14]. It is also worth noting that there is no ANE from Fe_3O_4 at 50 K as it is electrically insulating [41].

Since the SSE signal is dependent on the minor variations in the Pt layer thickness, we further normalize S_{J_Q} by the sheet resistance of the Pt layer R_s (measured using the four-probe technique and given in the SI) and define $S_{J_Q}^{R_s} = \frac{S_{J_Q}}{R_s}$. The variation of $S_{J_Q}^{R_s}$ with $t_{\text{Fe}_3\text{O}_4}$ is shown in Fig. 2(b) at 50 and 300 K. The decrease in SSE coefficient with temperature is consistent with previous reports [14].

We fit the variation of $S_{J_Q}^{R_s}$ with $t_{\text{Fe}_3\text{O}_4}$ to that predicted by the linear response theory (for direct comparison with [14]) given by [14,23]

$$S_{J_Q}^{R_s} \propto \frac{(1 - \text{sech}(\delta_{\text{FM}}))(1 - \text{sech}(\delta_{\text{NM}}))}{(\tanh(\delta_{\text{NM}}) + F_s)(\tanh(\delta_{\text{FM}}) + F_m) - G_s G_m}, \quad (3)$$

where $\delta_{\text{FM}} = \frac{t_{\text{Fe}_3\text{O}_4}}{\Lambda_{\text{Fe}_3\text{O}_4}}$, $\delta_{\text{NM}} = \frac{t_{\text{Pt}}}{\Lambda_{\text{Pt}}}$, Λ_{Pt} is the spin diffusion length of Pt, F_s , F_m , G_s and G_m are material constants. The fits were performed for F_m and $\Lambda_{\text{Fe}_3\text{O}_4}$ with $F_s = G_s = 5$, $G_m = 1$, $t_{\text{Pt}} = 5 \text{ nm}$, and $\Lambda_{\text{Pt}} = 7.7 \text{ nm}$ [42] and are shown in Fig. 2(b).

We obtained $\Lambda_{\text{Fe}_3\text{O}_4}^{300\text{K}} = 25.2 \pm 1.5 \text{ nm}$ and $\Lambda_{\text{Fe}_3\text{O}_4}^{50\text{K}} = 24.6 \pm 1.2 \text{ nm}$, which are equal within error. This would suggest that there is no change in the MDL with temperature, in contrast with previous measurements [14].

However, consideration of the in-plane magnetization should also be made due to its impact on the ISHE. The ISHE generated electric field is

$$\mathbf{E}_{\text{ISHE}} \propto \mathbf{J}_s \times \boldsymbol{\sigma}, \quad (4)$$

where \mathbf{J}_s is the spin current generated along the applied heat flux, in the direction of the surface normal. $\boldsymbol{\sigma}$ is the spin polarization of the conduction electrons in Pt, which is along the direction of the Fe_3O_4 layer magnetization \mathbf{M} [25]. We measured the in-plane saturation magnetic flux density $\mu_0 M_s$, at both 50 and 300 K as a function of $t_{\text{Fe}_3\text{O}_4}$ [shown in Fig. 2(c)]. We observed a variation similar to that of $S_{J_Q}^{R_s}$ and thus must be accounted for to extract the thickness dependence of the spin current \mathbf{J}_s . The inset of Fig. 2(c) shows the variation of the magnetic flux density $\mu_0 M$ with applied field at 300 K, showing the typical hysteretic behavior. A linear diamagnetic background has been subtracted from the datasets. The single-crystal value of $\mu_0 M_s$ at both 50 and 300 K is $\approx 0.6 \text{ T}$ [43] and we can see that for $t_{\text{Fe}_3\text{O}_4} > 40 \text{ nm}$, $\mu_0 M_s$ for the thin films approach this value. We observe a decrease in $\mu_0 M_s$ for lower $t_{\text{Fe}_3\text{O}_4}$ and expect that a decrease in $t_{\text{Fe}_3\text{O}_4}$ causes an out-of-plane canting of the magnetization and thus a decrease in the in-plane magnetization [44].

To account for the thickness dependence of $\boldsymbol{\sigma}$ introduced via the ISHE and $\mu_0 M_s$ in $S_{J_Q}^{R_s}$, we monitor the variation of $\frac{S_{J_Q}^{R_s}}{\mu_0 M_s}$ with $t_{\text{Fe}_3\text{O}_4}$ [shown in Fig. 2(d)], which from Eq. (4) is proportional to \mathbf{J}_s . We observe that while a decreasing trend for lower $t_{\text{Fe}_3\text{O}_4}$ is still evident at 300 K, it is considerably reduced at 50 K, indicating that there is a larger contribution from $\mu_0 M_s$ to the SSE response at this temperature. We also fit these trends (of the variation of $\frac{S_{J_Q}^{R_s}}{\mu_0 M_s}$ with $t_{\text{Fe}_3\text{O}_4}$) to that predicted by Eq. (3) [also shown in Fig. 2(d)] and obtained $\Lambda_{\text{Fe}_3\text{O}_4}^{300\text{K}} = 19.2 \pm 2.3 \text{ nm}$ and $\Lambda_{\text{Fe}_3\text{O}_4}^{50\text{K}} = 12.6 \pm 4.0 \text{ nm}$. These values show the same trend as the decreased MDL at low temperatures observed in YIG thin films which has been attributed to the reduction in the magnon thermal velocity with decrease in temperature [45]. We believe that these are accurate estimates of the MDLs in Fe_3O_4 thin films after accounting for the effect of the decrease in $\boldsymbol{\sigma}$ with decreasing film thickness. We have also fit the thickness variation of $\frac{S_{J_Q}^{R_s}}{\mu_0 M_s}$ to the exponential model described in Refs. [21,46] (more details can be found in the SI) and obtain similar values for $\Lambda_{\text{Fe}_3\text{O}_4}$ (within error).

The MDL values estimated from thin film SSE measurements are around half the values estimated from bulk single-crystal INS measurements. This could be a result of defects or due to the presence of a minor α -Fe phase (seen in the XRD spectrum in Fig. S3 in Ref. [32]) in the thin films, which can cause higher magnon scattering/damping and a lowering of the MDL. Nevertheless, INS measurements provide an upper limit on the expected MDL at 300 and 50 K. We also note that we find no evidence of the increase in MDL with decreasing temperature, which was reported in Ref. [14], from both INS and SSE estimates. We expect that some of the

trends observed in Ref. [14] are skewed by the uncertainties introduced by considering S_{VT} as the SSE coefficient.

In conclusion, we have measured the magnon dispersion in a single crystal of Fe_3O_4 using inelastic neutron scattering as a function of temperature and observe that the extracted MDLs $\Lambda_{\text{Fe}_3\text{O}_4}^{300\text{ K}} = 34.1 \pm 7.7$ nm and $\Lambda_{\text{Fe}_3\text{O}_4}^{50\text{ K}} = 27.2 \pm 5.7$ nm. We also measured the heat flux normalized SSE in $\text{SiO}_2/\text{Fe}_3\text{O}_4/\text{Pt}$ thin films and normalize by the static magnetization contribution to the SSE (introduced via the ISHE) before determining the MDLs $\Lambda_{\text{Fe}_3\text{O}_4}^{300\text{ K}} = 19.2 \pm 2.3$ nm and $\Lambda_{\text{Fe}_3\text{O}_4}^{50\text{ K}} = 12.6 \pm 4.0$ nm, which are smaller than that obtained from INS measurements. We hope that these studies will highlight the importance of disentangling the role of various effects in SSE measurements as well as motivate further studies to relate the SSE to the variation in $\mu_0 M_s$ and MDL in magnetic thin films.

All supporting data will be made available via the Loughborough data repository [47]. The MAPS data is available in Ref. [48]. The IN8 data is available in Ref. [49].

We would like to acknowledge the use of facilities and the assistance of Keith Yendall in the Loughborough Materials Characterisation Centre and Gavin Stenning in the Materials Characterisation Laboratory at the Rutherford Appleton laboratory. We also acknowledge the contributions of A. Sola and V. Basso from INRIM, Italy who helped develop the heat flux SSE measurement setup. We would like to thank T. Kuschel for useful discussions and feedback. Beamline experiments at the ISIS Neutron and Muon Source were supported by a beamtime allocation from the Science and Technology Facilities Council. This work was supported by the EPSRC Fellowship (EP/P006221/1).

-
- [1] K. Uchida, S. Takahashi, K. Harii, J. Ieda, W. Koshibae, K. Ando, S. Maekawa, and E. Saitoh, *Nature (London)* **455**, 778 (2008).
- [2] K. Uchida, M. Ishida, T. Kikkawa, A. Kirihara, T. Murakami, and E. Saitoh, *J. Phys. Condens. Matter* **26**, 343202 (2014).
- [3] G. E. Bauer, E. Saitoh, and B. J. Van Wees, *Nat. Mater.* **11**, 391 (2012).
- [4] K. Uchida, H. Adachi, T. Kikkawa, A. Kirihara, M. Ishida, S. Yorozu, S. Maekawa, and E. Saitoh, *Proc. IEEE* **104**, 1946 (2016).
- [5] E. S. Toberer, L. L. Baranowski, and C. Dames, *Annu. Rev. Mater. Res.* **42**, 179 (2012).
- [6] A. J. Caruana, M. D. Cropper, J. Zipfel, Z. Zhou, G. D. West, and K. Morrison, *Phys. Status Solidi-R* **10**, 613 (2016).
- [7] A. Chumak, V. Vasyuchka, A. Serga, and B. Hillebrands, *Nat. Phys.* **11**, 453 (2015).
- [8] A. Rastogi, Z. Li, A. V. Singh, S. Regmi, T. Peters, P. Bougiatioti, D. Carsten né Meier, J. B. Mohammadi, B. Khodadadi, T. Mewes, R. Mishra, J. Gazquez, A. Y. Borisevich, Z. Galazka, R. Uecker, G. Reiss, T. Kuschel, and A. Gupta, *Phys. Rev. Applied* **14**, 014014 (2020).
- [9] K. Uchida, H. Adachi, T. Ota, H. Nakayama, S. Maekawa, and E. Saitoh, *Appl. Phys. Lett.* **97**, 172505 (2010).
- [10] S. Bosu, Y. Sakuraba, K. Uchida, K. Saito, T. Ota, E. Saitoh, and K. Takanashi, *Phys. Rev. B* **83**, 224401 (2011).
- [11] C. D. W. Cox, A. J. Caruana, M. D. Cropper, D. M. Tatnell, C. J. Kinane, T. R. Charlton, and K. Morrison, in *Spintronics X* (International Society for Optics and Photonics, Bellingham, WA, 2017), Vol. 10357, p. 1035731.
- [12] Z. Zhang and S. Satpathy, *Phys. Rev. B* **44**, 13319 (1991).
- [13] X. Wang, Y. Liao, D. Zhang, T. Wen, and Z. Zhong, *J. Mater. Sci. Technol.* **34**, 1259 (2018).
- [14] A. Anadón, R. Ramos, I. Lucas, P. A. Algarabel, L. Morellón, M. R. Ibarra, and M. Aguirre, *Appl. Phys. Lett.* **109**, 012404 (2016).
- [15] R. Ramos, T. Kikkawa, M. H. Aguirre, I. Lucas, A. Anadón, T. Oyake, K. Uchida, H. Adachi, J. Shiomi, P. A. Algarabel, L. Morellón, S. Maekawa, E. Saitoh, and M. R. Ibarra, *Phys. Rev. B* **92**, 220407(R) (2015).
- [16] R. Ramos, A. Anadón, I. Lucas, K. Uchida, P. Algarabel, L. Morellón, M. Aguirre, E. Saitoh, and M. Ibarra, *APL Mater.* **4**, 104802 (2016).
- [17] R. Ramos, T. Kikkawa, A. Anadón, I. Lucas, K. Uchida, P. Algarabel, L. Morellón, M. Aguirre, E. Saitoh, and M. Ibarra, *AIP Adv.* **7**, 055915 (2017).
- [18] J. Xiao, G. E. W. Bauer, K. C. Uchida, E. Saitoh, and S. Maekawa, *Phys. Rev. B* **81**, 214418 (2010).
- [19] S. M. Rezende, A. Azevedo, and R. L. Rodríguez-Suárez, *J. Phys. D Appl. Phys.* **51**, 174004 (2018).
- [20] B. L. Giles, Z. Yang, J. S. Jamison, and R. C. Myers, *Phys. Rev. B* **92**, 224415 (2015).
- [21] A. Kehlberger, U. Ritzmann, D. Hinzke, E. J. Guo, J. Cramer, G. Jakob, M. C. Onbasli, D. H. Kim, C. A. Ross, M. B. Jungfleisch, B. Hillebrands, U. Nowak, and M. Kläui, *Phys. Rev. Lett.* **115**, 096602 (2015).
- [22] T. B. Noack, H. Y. Musiienko-Shmarova, T. Langner, F. Heussner, V. Lauer, B. Heinz, D. A. Bozhko, V. I. Vasyuchka, A. Pomyalov, V. S. Lvov, B. Hillebrands, and A. A. Serga, *J. Phys. D Appl. Phys.* **51**, 234003 (2018).
- [23] H. Adachi, J. I. Ohe, S. Takahashi, and S. Maekawa, *Phys. Rev. B* **83**, 094410 (2011).
- [24] V. Kalappattil, R. Das, M.-H. Phan, and H. Srikanth, *Sci. Rep.* **7**, 13316 (2017).
- [25] K. I. Uchida, J. I. Ohe, T. Kikkawa, S. Daimon, D. Hou, Z. Qiu, and E. Saitoh, *Phys. Rev. B* **92**, 014415 (2015).
- [26] B. N. Brockhouse and H. Watanabe, Spin waves in magnetite from neutron scattering, Tech. Rep. No. AECL-1575 (Atomic Energy of Canada Ltd., Chalk River, Ontario, Canada, 1962).
- [27] R. J. McQueeney, M. Yethiraj, W. Montfrooij, J. S. Gardner, P. Metcalf, and J. Honig, *Phys. Rev. B* **73**, 174409 (2006).
- [28] J. Barker and G. E. W. Bauer, *Phys. Rev. Lett.* **117**, 217201 (2016).
- [29] R. Ewings, A. Buts, M. Le, J. van Duijn, I. Bustinduy, and T. Perring, *Nucl. Instrum. Meth. A* **834**, 132 (2016).
- [30] S. Toth and B. Lake, *J. Phys. Condens. Matter* **27**, 166002 (2015).
- [31] M. Björck and G. Andersson, *J. Appl. Crystallogr.* **40**, 1174 (2007).

- [32] See Supplemental Material at <http://link.aps.org/supplemental/10.1103/PhysRevMaterials.4.075402> for further sample characterization and data analysis.
- [33] G. Venkat, C. D. W. Cox, A. Sola, V. Basso, and K. Morrison, [arXiv:2003.07925](https://arxiv.org/abs/2003.07925) [Rev. Sci. Instrum. (to be published)].
- [34] G. Venkat, T. Rose, C. D. W. Cox, G. B. G. Stenning, A. J. Caruana, and K. Morrison, *EPL* **126**, 37001 (2019).
- [35] A. Sola, V. Basso, M. Kuepferling, M. Pasquale, D. C. né Meier, G. Reiss, T. Kuschel, T. Kikkawa, K. Uchida, E. Saitoh, H. Jin, S. J. Watzman, S. Boona, J. Heremans, M. B. Jungfleisch, W. Zhang, J. E. Pearson, A. Hoffmann, and H. W. Schumacher, *IEEE T. Instrum. Meas.* **68**, 1765 (2018).
- [36] A. Sola, P. Bougiatioti, M. Kuepferling, D. Meier, G. Reiss, M. Pasquale, T. Kuschel, and V. Basso, *Sci. Rep.* **7**, 46752 (2017).
- [37] P. Bougiatioti, C. Klewe, D. Meier, O. Manos, O. Kuschel, J. Wollschläger, L. Bouchenoire, S. D. Brown, J. M. Schmalhorst, G. Reiss, and T. Kuschel, *Phys. Rev. Lett.* **119**, 227205 (2017).
- [38] C. D. W. Cox, A. J. Caruana, S. Davies, Z. Zhou, C. Kinane, B. Nicholson, A. Mora-Hernandez, A. Hindmarch, L. Bouchenoire, M. Cropper, and K. Morrison (unpublished).
- [39] C. Klewe, T. Kuschel, J.-M. Schmalhorst, F. Bertram, O. Kuschel, J. Wollschläger, J. Stempffer, M. Meinert, and G. Reiss, *Phys. Rev. B* **93**, 214440 (2016).
- [40] R. Ramos, T. Kikkawa, K. Uchida, H. Adachi, I. Lucas, M. H. Aguirre, P. Algarabel, L. Morellón, S. Maekawa, E. Saitoh, and M. R. Ibarra, *Appl. Phys. Lett.* **102**, 072413 (2013).
- [41] E. J. W. Verwey, *Nature (London)* **144**, 327 (1939).
- [42] H. Nakayama, K. Ando, K. Harii, T. Yoshino, R. Takahashi, Y. Kajiwara, K. Uchida, Y. Fujikawa, and E. Saitoh, *Phys. Rev. B* **85**, 144408 (2012).
- [43] Ö. Özdemir, *Geophys. J. Int* **141**, 351 (2000).
- [44] J. Nibarger, R. Lopusnik, Z. Celinski, and T. Silva, *Appl. Phys. Lett.* **83**, 93 (2003).
- [45] L. J. Cornelissen, J. Shan, and B. J. van Wees, *Phys. Rev. B* **94**, 180402(R) (2016).
- [46] E.-J. Guo, J. Cramer, A. Kehlberger, C. A. Ferguson, D. A. MacLaren, G. Jakob, and M. Kläui, *Phys. Rev. X* **6**, 031012 (2016).
- [47] G. Venkat, C. D. W. Cox, D. Voneshen, A. J. Caruana, A. Piovano, M. D. Cropper, and K. Morrison, Data cite for “Magnon diffusion lengths in bulk and thin film Fe₃O₄ for spin Seebeck applications”, doi: [10.17028/rd.lboro.2001261](https://doi.org/10.17028/rd.lboro.2001261) (2020).
- [48] doi: [10.5286/isis.e.rb1820362](https://doi.org/10.5286/isis.e.rb1820362).
- [49] doi: [10.5291/ILL-DATA.4-01-1576](https://doi.org/10.5291/ILL-DATA.4-01-1576).